Available online at www.sciencedirect.com
ScienceDirect
Journal of Sound and Vibration 309 (2008) 613–636
JOURNAL OF SOUND AND VIBRATION
www.elsevier.com/locate/jsvi

Snap loads and torsional oscillations of the original Tacoma Narrows Bridge

R.H. Plaut*

Department of Civil and Environmental Engineering, Virginia Polytechnic Institute and State University, Blacksburg, VA 24061, USA

Received 12 July 2006; received in revised form 21 February 2007; accepted 24 July 2007
Available online 21 September 2007

Abstract

In 1940, the original Tacoma Narrows Bridge was completed on June 10 and opened to traffic on July 1. On November 7, the deck collapsed. Before that day, significant vertical oscillations had occurred, but no torsion. The bridge as built was stable with respect to torsional motion under the winds of November 7 and previous winds with higher speeds. However, snap loads in the diagonal ties attached to the north midspan cable band helped to loosen the band, and the frictional resistance between the band and the north suspension cable passing through it was overcome. The cable began to slip through the band. For this new structural system, with longitudinal motion of the north cable, the wind speed was higher than the critical speed for torsional flutter, and torsional motion was initiated. Approximately 700 cycles of torsional oscillations occurred during the hour prior to the collapse. In the present study, the snap loads on the cable band are discussed first. Then a continuum model of the central span (deck, cables, and hangers) is formulated. The longitudinal motions of the cables are included, so that the slippage can be incorporated. Known information from the observed steady-state torsional motion is utilized with assumed forms of the vertical cable displacements, and the governing equations provide the horizontal cable displacements, the dynamic tensions in the cables, the vertical and torsional motions of the deck, and the resultant lift force and pitching moment (including damping) acting on the deck during its final hour.

1. Introduction

The collapse of the central span of the original Tacoma Narrows Bridge on November 7, 1940, has been studied extensively. A thorough report (the "Carmody Report") was written by a governmental committee consisting of O.H. Ammann, T. von Kármán, and G.B. Woodruff in 1941 [1]. Much information is also included in a five-part bulletin published during 1949–1954 [2–6]. Two excellent books are Scott [7] and Hobbs [8], and they list numerous references. Also, web sites from the Washington State Department of Transportation [9], University of Washington [10], and Tacoma Public Library [11] include interesting photos and facts.

Numerous physical and mathematical descriptions of the failure have been presented. The cause of the collapse has been a controversial subject, particularly with regard to the aerodynamic forces acting

*Tel.: +1 540 231 6072; fax: +1 540 231 7532.
E-mail address: rplaut@vt.edu

0022-460X/$ - see front matter
doi:10.1016/j.jsv.2007.07.057

on the bridge (e.g., Ref. [12]). Two aspects are considered here, the forces on the cable band whose failure led to the torsional motion of the deck, and the behavior of the central span during those torsional oscillations.

Clark Eldridge, a bridge engineer for the Washington State Toll Bridge Authority, proposed a design in 1938. The central span was 853.4 m (2800 ft) long and 11.9 m (39 ft) wide, with two lanes. A truss below the roadway was 7.6 m (25 ft) deep to stiffen the deck against vertical, lateral, and torsional displacements. The design was submitted to the US Public Works Authority (PWA), which was to provide a grant for 45 percent of the cost, with the remainder to be borrowed from the Reconstruction Finance Corporation and paid back from tolls. The estimated cost was $11 million. The PWA wanted to lower the cost, and a well-known consultant, Leon Moisseiff of New York, was hired. He replaced the truss in Eldridge's design with two vertical (stiffening) silicon-steel plate girders along the sides, extending 1.22 m (4 ft) above and below the roadway (Fig. 1) [7,9]. Stringers and laterals with a chevron (K) configuration were placed below the deck [1, p. 13]. The new estimated cost was $6.4 million. Even though at least one of the Washington State engineers said that the new design was "fundamentally unsound" [8], they accepted the new deck so that they could get a bridge over the Tacoma Narrows.

As an aside, a replacement bridge was built on the site 10 years after the collapse, for $14 million. It has four lanes. The deck is 18.3 m (60 ft) wide and 10.1 m (33 ft) deep, with a stiffening truss below the roadway and with three sets of diagonal shock absorbers on each side at midspan. An adjacent bridge with three lanes opened in 2007, at a cost of $849 million.

The original bridge exhibited significant vertical oscillations during the 5 months between its completion and its collapse. Wind speeds reached above 22 m/s (50 mph) [1, p. 28]. The largest reported amplitude of the vertical motion from equilibrium was 0.76 m (2.5 ft), although Professor F.B. Farquharson of the University of Washington, who was a frequent observer at the bridge, was skeptical of this value [2]. Amplitudes of 0.4 m (1.4 ft) were often recorded.

On November 7, 1940, a wind speed of 19 m/s (42 mph) was measured at the eastern end of the bridge, although the speed may have been higher on other parts of the bridge and at other times during the morning [13]. The wind was southerly and hit the bridge obliquely. The motion of the deck before 10 a.m. was vertical with an amplitude not more than 0.5 m (1.5 ft) and had eight or more nodes in the central span [2]. (The form of the motion was determined with the use of a transit on top of the toll house on the eastern end of

Fig. 1. Torsional motion on November 7, 1940 (from Ref. [9], with permission from Washington State Department of Transportation; GHPHSM, Bashford 2784).

the bridge, targets on the lampposts, and a fixed target on the eastern tower.) The frequency of the motion was 36–38 cycles per second (0.60–0.63 Hz), which was significantly higher than previously reported frequencies [2].

Around 10 a.m., the motion switched into a torsional mode with a node at midspan (Fig. 1). The initial frequency was 14 cycles per minute (0.23 Hz), but after a short time it decreased to 12 cycles per minute (0.2 Hz), perhaps due to some damage within the deck [3,14]. Although the motion of the central span changed form somewhat during the subsequent hour, it was primarily a one-noded torsional oscillation. After examining the films, Farquharson concluded that the maximum twist angle was about 35°, corresponding to a maximum vertical amplitude of approximately 4.3 m (14 ft) along the edge of the deck [2,8]. The central span collapsed around 11 a.m. and fell into the Tacoma Narrows [7,8,15].

Torsional oscillations had not been observed on the bridge prior to its last hour. They occurred because of a change in the structure: loosening of the north midspan cable band. This event will be discussed in the next section. It involves snap loads in the diagonal ties that were attached to the cable band. Then the ensuing steady-state torsional motion will be considered. In Section 3, a continuum model of the central span will be formulated. It will be more general than previous models, involving the longitudinal motions of the cables that occurred after the frictional resistance in the band was overcome. Results will be presented in Section 4. Approximate solutions will be obtained for the displacements of the deck and cables, the forces in the cables, and the resultant vertical force and pitching moment acting on the deck. Concluding remarks will be given in Section 5.

2. North midspan cable band

2.1. Behavior before torsional motion occurred

Hanging from each of the two main suspension cables connecting the two towers were 55 sets of four vertical hangers (suspenders), spaced 15.2 m (50 ft) apart. Fig. 2 is a photograph, taken during construction, of one of the sets of hangers at midspan, along with two diagonal ties (stays, guys). The hangers consisted of two wire ropes that looped over a cable band (sheath, collar) and were attached to the top of the plate girder.

Fig. 2. Diagonal ties and midspan cable band (from Washington State Archives, with permission).

The diagonal ties were placed at the midspan cable band to reduce relative longitudinal motions between the cable and the deck, and to prevent torsional motion of the deck [6]. As long as the friction between the band and the cable kept the cable from slipping through the band (i.e., until 10 a.m. on November 7), the diagonal ties were effective [16].

The cable bands were made of welded steel for the first time in a suspension bridge, and were lighter than the normal ones made of cast steel [7,13,17]. The two semi-cylindrical halves, one on each side of the cable, were connected by three horizontal bolts at the top and three at the bottom. The bolts were initially tightened to a tensile stress of 360 MPa (52 ksi), and were checked and tightened periodically [18] since bolt loads tend to relax [19].

The hangers were 7×7 galvanized steel ropes with a diameter of 3.2 cm (1.25 in.) [20]. They rested on a heavy paste in grooves at the top of the cable band [18]. The upper part of the diagonal ties was galvanized steel bridge strand with a diameter of 3.8 cm (1.5 in.) [4]. The ties were attached underneath the cable band with lugs, and to the top of the plate girder with clips [1, p. 16]. A turnbuckle between the bridge strand and the plate girder allowed for the tension to be adjusted, but unfortunately only nominal pretension was applied to the ties [1, p. 55].

The cables had a diameter of 0.44 m (1.44 ft). They consisted of 19 parallel strands of 332 No. 6 galvanized cold-drawn steel wires. Between adjacent bands, the cables were tightly wrapped circumferentially with No. 9 soft annealed and double-galvanized wire, to make them smooth and waterproof [4,13].

Before 10 a.m. on November 7, W.F. Miles of the Pacific Bridge Company noted that the diagonal ties attached to the north midspan cable band were alternately becoming slack and taut [1, p. V-14]. A short part of his film of this behavior is located at the Special Collections Division of the University of Washington. Two still pictures from the film, taken at approximately 9:40 a.m., are shown in Fig. 3. The tie is taut in the top picture and slack in the bottom one. This action resulted in snap loads being applied to the cable band (i.e., impact-like forces when a tie became taut), in alternating directions longitudinally [1, p. 31]. These snap loads apparently helped cause the cable band to become loose.

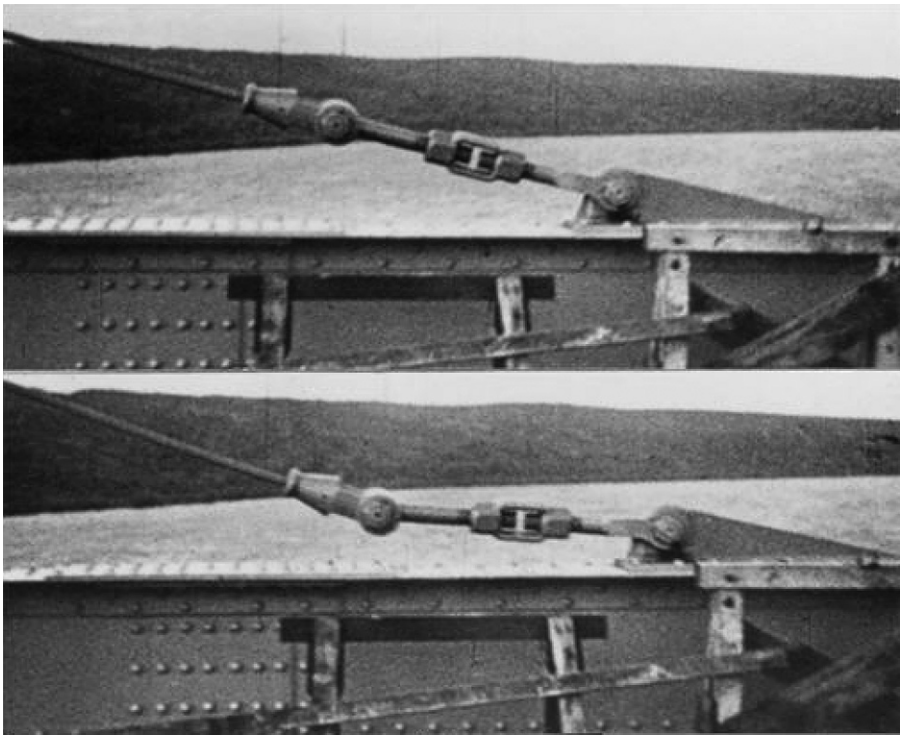

Fig. 3. Taut (top) and slack (bottom) conditions of midspan tie just before torsion (with permission from University of Washington Libraries, Special Collections, Negative number UW26370).

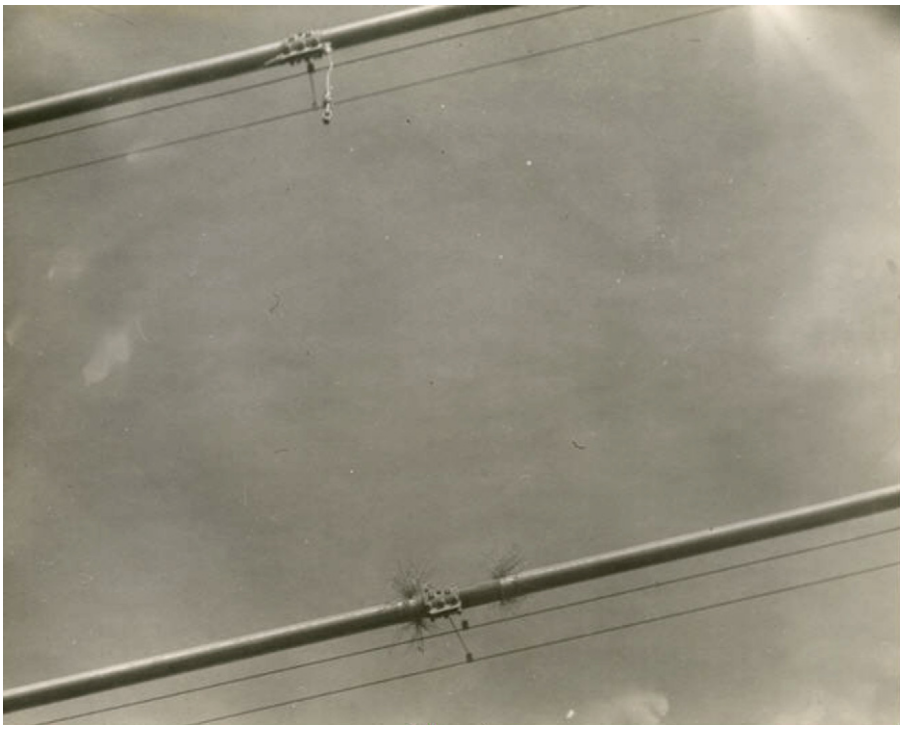

Fig. 4. North (bottom) and south (top) midspan cable bands after deck collapse (from Richard S. Hobbs, with permission from Washington State Archives).

Starting around 10 a.m., the north cable began slipping through the midspan band back and forth with an amplitude of 0.51 m (1.67 ft) [1, p. 57]. The wrapping was pushed aside, and 351 of the 6308 wires in the cable broke, mostly near the top of the cable [13]. Fig. 4 is a photo of the midspan cable bands after the bridge collapsed. Some of the broken wires can be seen on the north cable, at the bottom of the figure, whereas the south cable band shows no evidence of cable slippage. A close-up photo of one set of broken wires on the north cable is shown in Fig. 5.

The importance of the slippage can be seen in Fig. 6 [21], a sketch of possible cable and deck displacements (dashed curves) along the north edge of the deck. For one-noded torsional motion, one half of the edge (on the left of the figure) will tend to move downward and the other half will tend to move upward, for example. The cable above the edge will tend to do the same. If the ends of the cable at the towers do not move, the arc length of the cable on the left side between the tower and midspan wants to increase, whereas the arc length on the right side wants to decrease. Hence the midpoint of the cable wants to move to the left in the figure, from c to c'. The cable on the other edge of the deck tends to move in the opposite direction as the deck twists about its centerline. When both midspan cable bands in the bridge restrain the cables from such slippage, torsional motion is prevented or at least hindered.

2.2. Models of snap loads on cable band

In this subsection, the longitudinal (horizontal) forces on the north midspan cable band, before slippage occurred, are considered. Fig. 7 is a sketch of the band, the left diagonal tie, the hangers passing over the band, and a section of cable (shaded). Based on the plan for the bridge, the dimensions are $L_w = 2.1$ m (6.8 ft), $L_s = 4.0$ m (13.2 ft), $D_s = 4.8$ m (15.7 ft), $L_o = 1.5$ m (5.0 ft), and $L_B = 0.7$ m (2.3 ft). Various mathematical models can be used to try to represent the effects of the snap loads on the band.

The single-degree-of-freedom system shown in Fig. 8 is considered in this section. A mass m is subjected to harmonic forcing $P\sin(\Omega T - \psi)$, where T denotes time, and the resulting motion is $U(T)$. The ties are assumed

Fig. 5. Broken cable wires at north midspan cable band (from Ref. [9], with permission from Washington State Department of Transportation).

to have no pretension, so the left tie is active (taut) when $U>0$ and its restoring (tension) force is F_L. The case of tension here can be related to the opposite case of impacts between two bodies [22,23], and hence F_L is depicted on the right side of the figure as if it represented a compressive force. Models such as that in Fig. 8 have been considered in many papers, including Refs. [24–26]. Periodic motions with period $2\pi/\Omega$ are of interest here. It is assumed that $U(0)=0$ and $V_o>0$, where V_o is the initial velocity. Results for the first half-cycle can then be utilized directly to obtain the motion for the second half-cycle, during which the active tensile force from the right tie is denoted F_R.

When $U>0$, the equation of motion is assumed to have the form

$$m\frac{\mathrm{d}^2U}{\mathrm{d}T^2}+C_L\frac{\mathrm{d}U}{\mathrm{d}T}+K_LU+K_NU^{1.5}\left(1+\frac{c_N}{V_o}\frac{\mathrm{d}U}{\mathrm{d}T}\right)=P\sin(\Omega T-\psi). \tag{1}$$

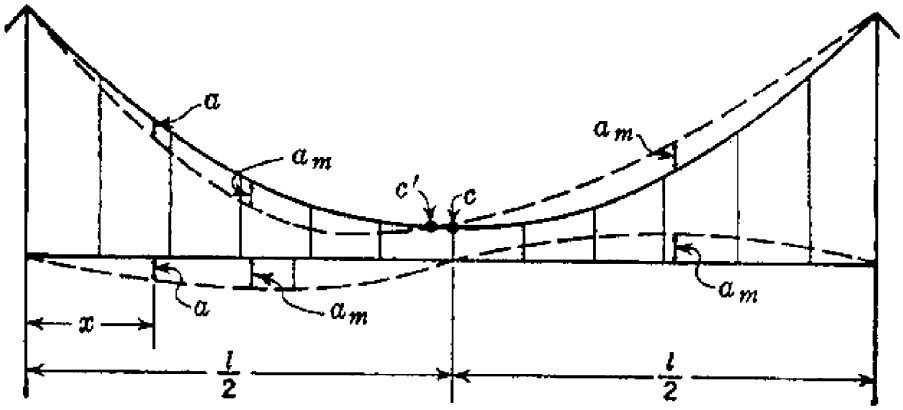

Fig. 6. Cable and hanger deformations during torsion (from Ref. [21], with permission from ASCE).

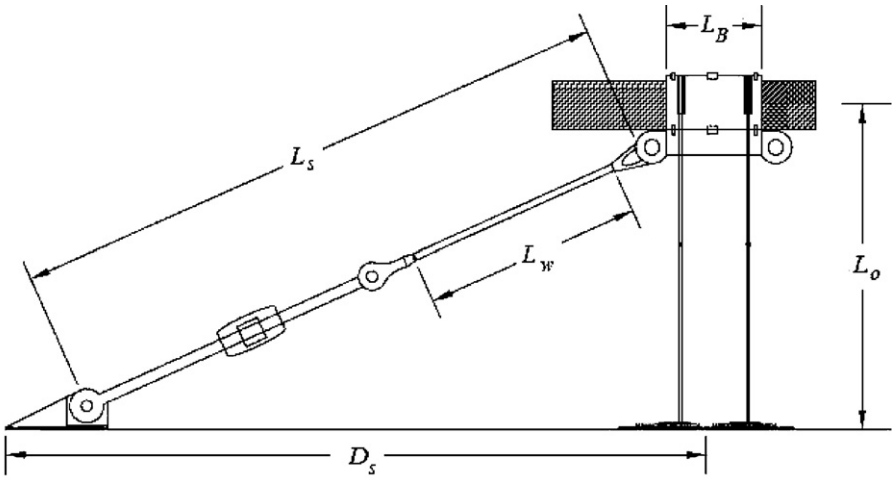

Fig. 7. Sketch of midspan cable band and one diagonal tie.

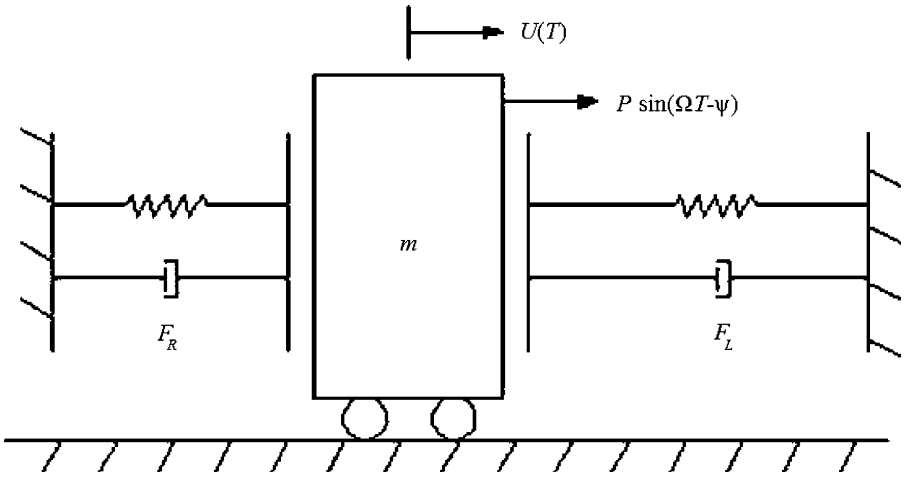

Fig. 8. Single-degree-of-freedom model for snap loads on cable band.

where C_L is a linear viscous damping coefficient, K_L is a linear stiffness coefficient, and K_N and c_N are parameters in a nonlinear coupled term that involves both displacement and velocity. The second, third, and fourth terms in Eq. (1) represent possible forms for F_L.

The following quantities are defined:

$$\alpha = \sqrt{\frac{K_L}{m}}, \quad t = \alpha T, \quad \omega = \frac{\Omega}{\alpha}, \quad p = \frac{P}{K_L - m\Omega^2}, \tag{2a–d}$$

$$u = \frac{U}{p}, \quad \zeta = \frac{C_L}{2\sqrt{K_L m}}, \quad k_N = \frac{K_N\sqrt{p}}{K_L}, \quad f_L = \frac{F_L}{K_L - m\Omega^2}. \tag{2e–h}$$

Then Eq. (1) can be written in the nondimensional form

$$\frac{d^2u}{dt^2} + 2\zeta\frac{du}{dt} + u + k_N u^{1.5}\left(1 + \frac{c_N}{v_o}\frac{du}{dt}\right) = (1-\omega^2)\sin(\omega t - \psi). \tag{3}$$

The first case discussed is called Case I. Short impacts are sometimes represented via a coefficient of restitution r. For example, in Ref. [27] the snap load of a cable was assumed to instantaneously reverse the sign of the velocity, so that just after the taut phase the velocity was $-r$ times the velocity just before it. Here, the velocity does not change sign at $T = 0$, so the velocity just after $T = 0$ is assumed to be r times the velocity just before $T = 0$ (as with the impacts in Ref. [28]). In Case I it is assumed that $\zeta = 0$ and $k_N = 0$, i.e., the second and fourth terms in Eq. (3) are deleted, so that the only loss of energy occurs at the slack/taut transition twice a cycle, once for the left tie and once for the right tie.

With the use of the conditions $u(0) = 0$, $u(\pi/\omega) = 0$, and $v(\pi/\omega) = -v_o/r$, where $v = du/dt$ and v_o is the nondimensional velocity just after $t = 0$, the solution of Eq. (3) for $0 < t < \pi/\omega$ (the first half-cycle) is

$$u(t) = \sin\psi\cos t - \frac{[1+\cos(\pi/\omega)]}{\sin(\pi/\omega)}\sin\psi\sin t + \sin(\omega t - \psi). \tag{4}$$

In Eq. (4), the phase ψ is computed from

$$\tan\psi = \frac{(1-r)\omega\,\sin(\pi/\omega)}{(1+r)[1+\cos(\pi/\omega)]}. \tag{5}$$

Numerical results for Case I are presented in Fig. 9 for the parameters $\omega = 0.8$, $r = 0.8$, and $v_o = 0.6953$, which yield $\psi = -0.2114$. The time history of the displacement is shown in Fig. 9(a). In the velocity history in Fig. 9(b), there is a jump in the magnitude of velocity from 0.8691 to 0.6953 at $t = 0$ and $t = 3.93 = \pi/\omega$. The phase plane in Fig. 9(c) shows the discontinuities in the velocity when $u = 0$, and the force–displacement plot in Fig. 9(d) is just a straight line through the origin, since the only loss of energy is due to the discontinuity in velocity.

The second model to be considered, Case II, involves a discontinuous force rather than a discontinuous velocity. Again the effect of the slack/taut transition is assumed to be instantaneous. A spring and a dashpot are used here, so that only the fourth term in Eq. (3) is deleted, i.e., $k_N = 0$. The dashpot causes a sudden force when the tie becomes taut at $t = 0$. In order to prevent a sudden change of force when the taut tie becomes slack, it is assumed that the dashpot is only active when the tie is elongating. When $u > 0$, therefore, $\zeta > 0$ if $v > 0$, and $\zeta = 0$ when $v < 0$.

Let t_1 denote the time during the first half-cycle at which $v = 0$ and the dashpot becomes inactive. Eq. (3) can be solved analytically for $0 < t < t_1$ and for $t_1 < t < \pi/\omega$, with u and v continuous at $t = t_1$, $u(0) = u(\pi/\omega) = 0$, and $v(\pi/\omega) = -v_o$. For the parameters $\omega = 0.8$ and (for $0 < t < t_1$) $\zeta = 0.02$, a numerical solution was obtained using Mathematica [29]. The results were $v_o = 0.7855$, $\psi = -0.04318$, and $t_1 = 1.9636 = 0.50003\pi/\omega$. Plots analogous to those in Fig. 9 are presented in Fig. 10. In this case, the displacement and velocity are continuous, and the force–displacement relationship in Fig. 10(d) exhibits a hysteresis loop with a discontinuity of 0.0314 in the force during each half-cycle (as seen in the magnified version of the behavior at the origin, shown in the inset).

Finally, Case III involves a tie force with a coupling between displacement and velocity. Similar forces dealing with impacts have been considered before, e.g., in Refs. [30–34]. Refs. [30,34] utilized the exponent 1.5

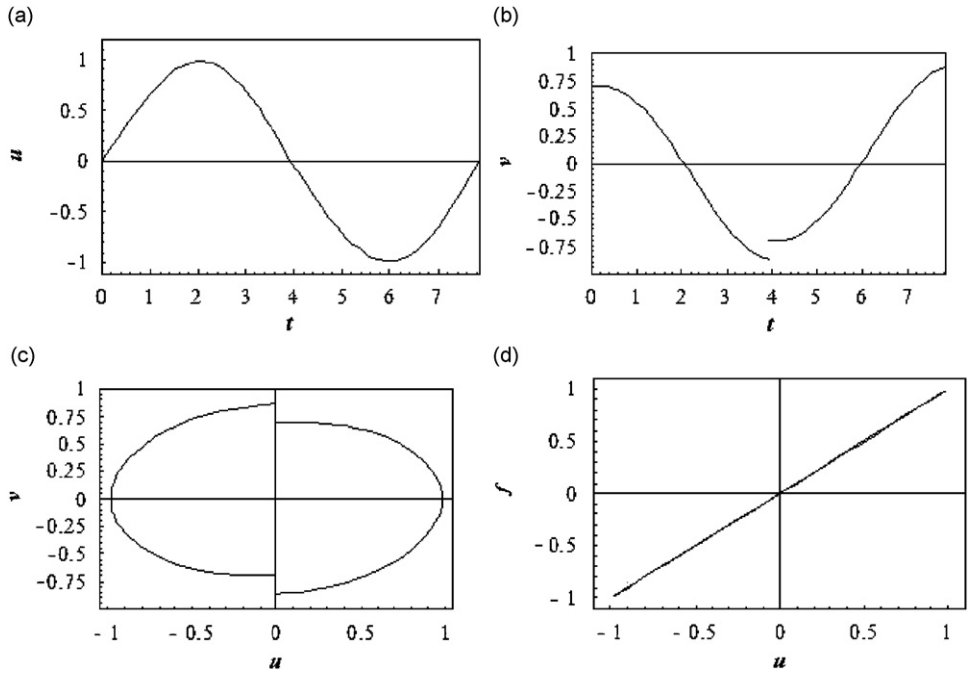

Fig. 9. Steady-state response of single-degree-of-freedom model with spring and coefficient of restitution: (a) displacement vs. time; (b) velocity vs. time; (c) velocity vs. displacement; and (d) force vs. displacement.

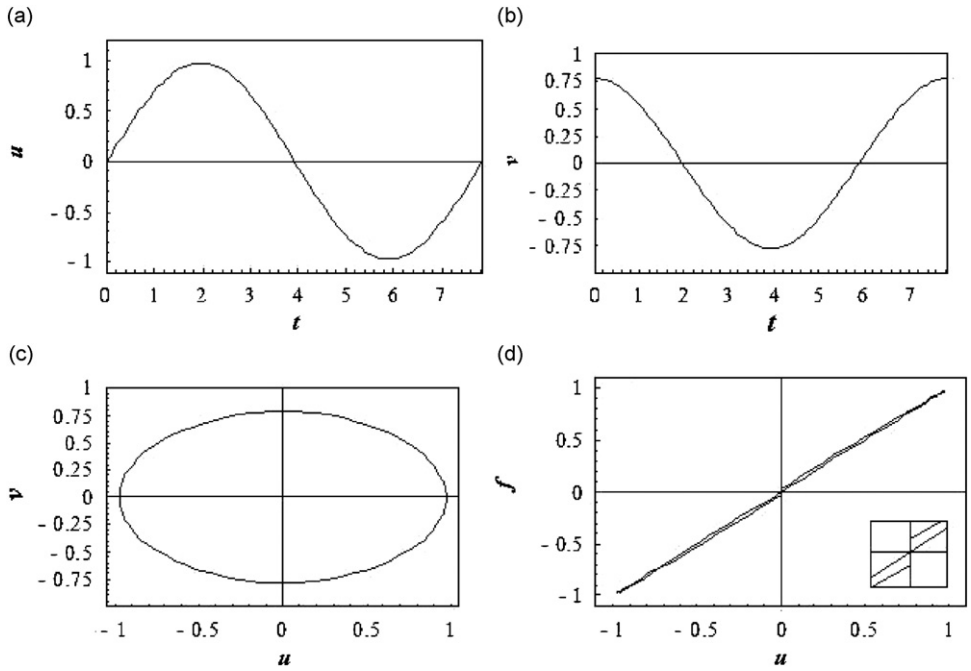

Fig. 10. Steady-state response of single-degree-of-freedom model with spring and (while elongating) dashpot: (a) displacement vs. time; (b) velocity vs. time; (c) velocity vs. displacement; and (d) force vs. displacement.

on the displacement, as in Eq. (3), based on the Hertz contact law from elasticity. Neither the velocity nor the force is discontinuous in this model. During static or dynamic elongation, wire ropes tend to stiffen, and this property is modeled here.

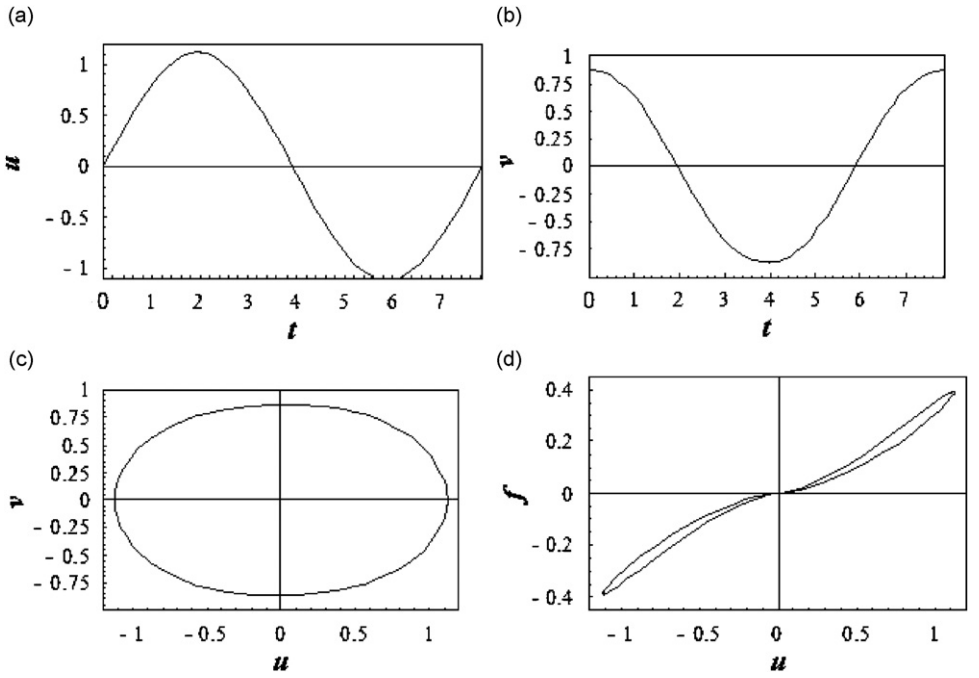

Fig. 11. Steady-state response of single-degree-of-freedom model with nonlinear coupled tie force: (a) displacement vs. time; (b) velocity vs. time; (c) velocity vs. displacement; and (d) force vs. displacement.

The subscript L is replaced by N in Eqs. (2), and the second and third terms in Eq. (3) are deleted. Eq. (3) was then solved numerically for the conditions $\omega = 0.8$, $c_N = 0.15$, $u(0) = 0$, $v_o = 0.8691$, and $v(\pi/\omega) = -v_o$. The numerical solution yields $k_N = 0.3279$ and $\psi = -3.0911$. The results are plotted in Fig. 11. Similar force–displacement hysteresis loops have been obtained experimentally from drop tests with parachute lines [35], drop tests with synthetic fiber ropes [36], and vibration tests with synthetic fiber ropes that exhibited slack and taut phases [37].

For the remainder of this paper, a continuum model of the central span will be formulated and then analyzed under the conditions of steady-state torsional oscillations existing during the last hour of the original Tacoma Narrows Bridge.

3. Previous continuum models of central span

Some papers that have considered section models of the Tacoma Narrows Bridge (i.e., motion of a cross section) are listed in Ref. [38]. Here, some of the studies utilizing continuum models of the central span are described. In this section, the coordinate along the deck is denoted x, time is t, the vertical motion of the centerline of the deck is $y(x, t)$, the torsional motion of the deck about the centerline is $\theta(x, t)$, and the vertical motions of the cables are $z_1(x, t)$ and $z_2(x, t)$ if there is torsion of the deck, and $z(x, t)$ if there is no torsion.

3.1. Vertical motion of deck: $y(x, t)$

Lazer and McKenna [39] considered the deck as a beam and the hangers as an elastic continuum (Winkler foundation) that only acted in tension. Hence the equation of motion for $y(x, t)$ was nonlinear, and multiple periodic solutions could exist when the beam was subjected to a distributed vertical force that varied harmonically over time. Subsequent analyses of this nature include Refs. [40–49]. Discussions of the Lazer–McKenna conjecture that slack/taut behavior of the hangers was important to the collapse of the bridge include Refs. [50,51].

3.2. Vertical motions of deck and cables: $y(x, t)$ and $z(x, t)$

Lazer and McKenna [39] also analyzed a model including coupled equations of motion for $y(x, t)$ and $z(x, t)$, assuming no rotation of the deck. The cables were treated as strings, with no bending stiffness, and again the hangers were assumed to exhibit slack/taut behavior. A vertical harmonically varying force was applied to the cables, and multiple periodic solutions were demonstrated. Related papers include Refs. [41,52–58].

3.3. Torsional motion of deck: $\theta(x, t)$

Moore [59] considered torsional motions $\theta(x, t)$, assuming uniform (St. Venant) torsion and an applied moment that varied harmonically in time. The hangers were assumed to remain taut. It was shown that multiple periodic solutions may exist.

3.4. Vertical and torsional motions of deck: $y(x, t)$ and $\theta(x, t)$

Jacover and McKenna [60] analyzed coupled equations for $y(x, t)$ and $\theta(x, t)$, with the bilinear hanger behavior as described in Section 3.1. The equation for torsional motion included the nonuniform (warping) torsion term, but not the uniform torsion term. Harmonically varying forces and moments were applied along the beam. Again, multiple solutions were obtained. Ahmed and Harbi [61] included uniform and nonuniform torsion terms, and Moore [62] assumed uniform torsion. Numerous papers have studied flexural–torsional motions of suspension bridges without invoking slack/taut behavior of the hangers, such as Refs. [63,64].

3.5. Vertical and torsional motions of deck, and vertical motions of cables: $y(x, t)$, $\theta(x, t)$, $z_1(x, t)$, and $z_2(x, t)$

Diaferio and Sepe [65] formulated four coupled equations of motion for $y(x, t)$, $\theta(x, t)$, $z_1(x, t)$, and $z_2(x, t)$. Uniform torsion was assumed, and a smooth nonlinear force was used to approximate the bilinear (slack/taut) model of the hangers described previously. Numerical solutions were only presented for the special cases of Sections 3.2 and 3.4 above, i.e., first with $\theta(x, t) = 0$ and $z_1(x, t) = z_2(x, t)$, and then with $z_1(x, t) = z_2(x, t) = 0$.

3.6. Summary and present approach

The hangers of the Tacoma Narrows Bridge probably remained in tension during the torsional oscillations [66]. Also, the switch from vertical to torsional motions occurred because of a change in the system, not because of a change from one steady-state solution to another in a given system, and not because of some particular disturbance or increase in excitation. Therefore, the analyses in many of the references cited above in Sections 3.1–3.5 may not be directly relevant to the collapse of the original Tacoma Narrows Bridge.

The analysis to be presented in the following section does not assume mathematical forms to represent the effects of the wind and structural damping on the torsional oscillations. Many papers have discussed the aerodynamic forces on the original Tacoma Narrows Bridge, including Refs. [67–74]. Most models assume that the displacements and velocities about the equilibrium state are small (e.g., that the square of the twist angle θ is negligible compared to unity). A nonlinear term of the van der Pol type, proportional to the product of θ^2 and the angular velocity, was included in Refs. [75–77]. Large motions will be allowed here. The cable motions and tensions, deck motions, and resultant vertical force and pitching moment acting on the deck during the torsional oscillations will be determined, based on the observed behavior of the bridge during its final hour.

4. Formulation of new continuum model of central span

4.1. Assumptions

Fig. 12 depicts a sketch of the side view of the bridge, not showing the diagonal ties and only showing some of the 55 sets of hangers on one side. Fig. 13 shows a perspective of the span.

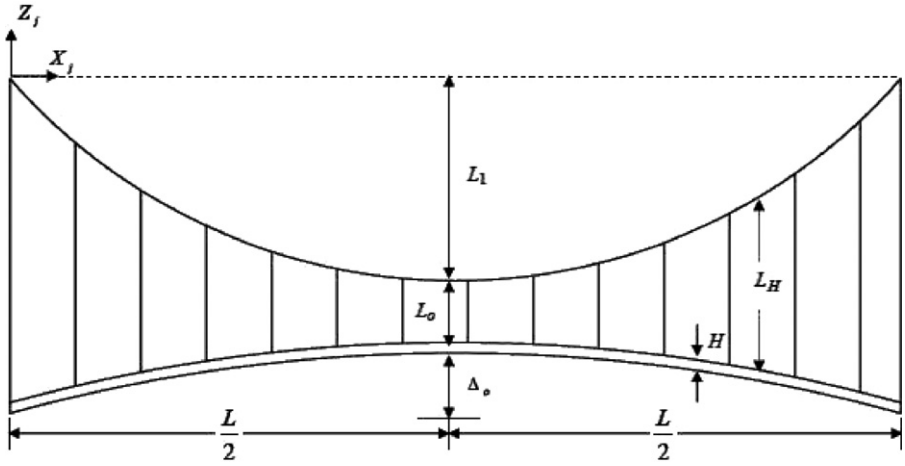

Fig. 12. Side view of central span.

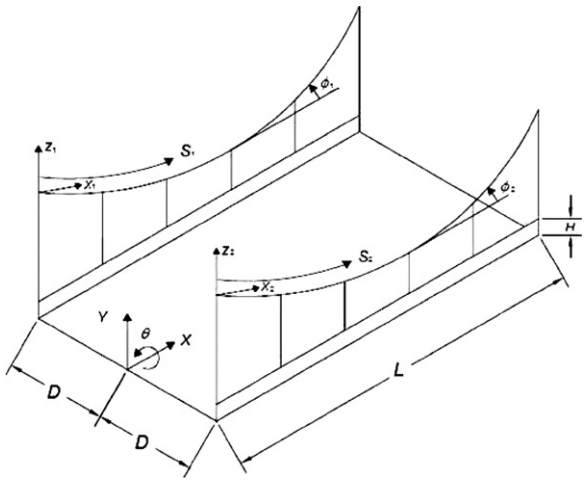

Fig. 13. Perspective view of central span.

During the torsional motion, it was observed (e.g., Fig. 1) that the side spans tended to be relatively quiet [1, p. 31], and the effects of their motions are not considered. It is assumed that the weight of the deck in the central span is carried by the two cables, i.e., contributions from the towers and the shear forces from the side spans are neglected; this is a common assumption for suspension bridges [78]. At the tops of the towers, the cables pass over saddles that have a horizontal length of 34.2 m (13.8 ft) [79], and it is assumed that the cables do not slip over the saddles. Longitudinal motions of the deck were reduced by the actions of hydraulic jacks (buffers, dampers) located at the towers [1, p. 16] and by the ties at midspan, and such motions are neglected here. The maximum lateral motion of the deck during the torsional oscillations was reported to be about 0.6 m (2 ft) [1, p. 49], which is small compared to the span length of 853.4 m (2800 ft); lateral motions of the deck, hangers, and cables are neglected.

The snap loads that were important in the initiation of the torsional motion are not included in this steady-state dynamic analysis, nor are friction forces between the cable bands and the cables. According to Ref. [1, p. 57], for cable 2, when the motion made the transition from vertical to torsional, "the resistance of the band practically disappeared" and the cable slipped freely back and forth through the band. With regard to cable 1, it is assumed in the present analysis that it has no longitudinal motion at its midspan band.

The cables are assumed to be linearly elastic and inextensible, as is normally done [78], although the inextensibility assumption is slightly relaxed in the numerical solution of the governing equations. The bending stiffness of the cables is neglected. The hangers are modeled as a linearly elastic continuum, as in many of the previous analyses, and here the hangers remain in tension during the oscillations. Their stiffness is based on the equilibrium length (i.e., L_H in Fig. 12), and their weight and inertia are not considered.

Wind and damping forces on the cables and hangers are neglected. Due to the camber of the deck, the wind from the south naturally causes some tilting of the deck such that the north side is lower than the south side (in the absence of torsional motion), but this effect is ignored. The deck is modeled as a uniform, homogeneous, linearly elastic, Euler–Bernoulli beam with an H-shaped cross section. The vertical motion of the centerline (but not the edges) is assumed to be small, i.e., the square of its slope along the centerline, relative to its slope at equilibrium, is negligible compared to unity. A nonlinear torsion term is included in the equation of motion for the twist angle [80], along with linear uniform and nonuniform torsion terms.

The following features are included in the continuum model: (a) The twist angle is allowed to be large, due to the inclusion of the nonlinear torsion term. In addition, another approximate pitching moment is computed by neglecting the deck's torsional resistance, showing that much of the resistance to torsion is due to the hanger-cable system and the rotational inertia, as previously claimed in Refs. [4,67,81]. (b) Motions of the cables are allowed to be large, as well as the dynamic tension forces in the cables. (c) There is no restriction on the size of the damping or aerodynamic forces, whose combined form is determined rather than assumed. (d) Both transverse and longitudinal inertias of the cables are included. (e) Slippage of the north cable through the midspan cable band is modeled. (f) The camber of the deck is included. (g) The stiffness of the hangers is not assumed to be constant along the span, unlike some previous studies. (h) Per unit length along the span, the weight of each cable is about one-sixth of the weight of the deck. For equilibrium, the weights of the cables and the deck are included, so that the shape of the cables is neither a parabola (as it would be without cable weight) nor a catenary (as it would be without deck weight) [82].

4.2. Parameters and variables

The width of the deck is denoted $2D$, the length of the central span is L, the equilibrium length of each cable between the towers is L_C, the height of the plate girders is $2H$, the difference between the midspan height of the deck and its height at the towers is Δ_o, the equilibrium height of the cable centerlines above the top of the plate girders at midspan is L_o, the sag of the cables is L_1, the weight of the deck per unit length along the span is W_D, the weight of a cable per unit length is W_C, the modulus of elasticity of the deck is E_D, the moment of inertia of the deck cross section with respect to a horizontal line through its centroid is I_D, the polar mass moment of inertia of the deck is I_P, the warping constant of the deck is I_w, the shear modulus of the deck is G_D, the torsional constant of the deck is J_D, the nonlinear Wagner constant of the deck is I_n [80], the effective modulus of elasticity of the cables is E_C, the effective modulus of elasticity of the hangers is E_H, the effective cross-sectional area of each hanger is A_H, the effective cross-sectional area of each cable is A_C, and the frequency of torsional oscillations is Ω. The values of these parameters are assumed to be [1,2,83,84]

$$
\begin{aligned}
D &= 5.94\,\text{m}\,(19.5\,\text{ft}), \quad L = 853.4\,\text{m}\,(2800\,\text{ft}), \quad L_C = 868.7\,\text{m}\,(2850\,\text{ft}),\\
H &= 1.22\,\text{m}\,(4\,\text{ft}), \quad \Delta_o = 5.5\,\text{m}\,(18\,\text{ft}), \quad L_o = 1.5\,\text{m}\,(5\,\text{ft}), \quad L_1 = 70.7\,\text{m}\,(232\,\text{ft}),\\
W_D &= 2734\,\text{kN/m}\,(4270\,\text{lb/ft}), \quad W_C = 458\,\text{kN/m}\,(715\,\text{lb/ft}),\\
E_D &= 200\,\text{GPa}\,(29\times10^6\,\text{lb/in.}^2), \quad I_D = 0.154\,\text{m}^4\,(17.8\,\text{ft}^4),\\
I_P &= 106,500\,\text{N s}^2\,(23,940\,\text{lb sec}^2), \quad I_w = 5.44\,\text{m}^6\,(6780\,\text{ft}^6),\\
G_D &= 80\,\text{GPa}\,(11.6\times10^6\,\text{lb/in.}^2), \quad J_D = 6.07\times10^{-6}\,\text{m}^4\,(7.03\times10^{-4}\,\text{ft}^4),\\
I_n &= 528\,\text{m}^6\,(657,900\,\text{ft}^6), \quad E_C = E_H = 185\,\text{GPa}\,(27\times10^6\,\text{lb/in.}^2),\\
A_H &= 6.4\,\text{cm}^2\,(0.99\,\text{in.}^2), \quad A_C = 0.123\,m^2\,(191.3\,\text{in.}^2), \quad \Omega = 1.26\,\text{rad/s}.
\end{aligned}
\tag{6}
$$

The value used for E_C and E_H is conventional in the design of suspension bridges, according to Ref. [2], and the cables and hangers are assumed to have an air void of approximately 20% in the calculation of their

effective areas [1,2,85]. The value of I_n is computed using the formula in Ref. [80] for a doubly symmetric I section. For the flanges of the I section, representing the plate girders, the thickness is 1.3 cm (0.5 in.) and the width is 2.4 m (8 ft). For the web (i.e., the roadway), the effective thickness is assumed to be 0.15 m (0.5 ft) and the width is 12 m (39 ft). Due to the stiffness of the deck, the resisting moment M_D about the centerline, including terms for uniform, nonuniform, and nonlinear torsion, is assumed to be [80]

$$M_D = G_D J_D \frac{\partial \theta_d}{\partial X} - E_D I_w \frac{\partial^3 \theta_d}{\partial X^3} + \frac{1}{2} E_D I_n \left(\frac{\partial \theta_d}{\partial X}\right)^3. \tag{7}$$

In Eq. (7), θ_d is the twist angle relative to equilibrium.

In Figs. 12 and 13, cable 1 is the south cable and cable 2 is the north cable. For cable j, in the vertical plane, at arc length S_j from the top of the left tower, the rotation is $\phi_j(S_j, T)$ and the coordinates are $X_j(S_j, T)$ and $Z_j(S_j, T)$, where T is time and the positive senses are shown in the figures. The tension in cable j is $N_j(S_j, T)$. Letting subscripts e and d denote equilibrium and dynamic values, respectively, these variables are written in the component form

$$\begin{gathered} X_j(S_j, T) = X_e(S_j) + X_{jd}(S_j, T), \quad Z_j(S_j, T) = Z_e(S_j) + Z_{jd}(S_j, T), \\ \phi_j(S_j, T) = \phi_e(S_j) + \phi_{jd}(S_j, T), \quad N_j(S_j, T) = N_e(S_j) + N_{jd}(S_j, T)\,(j = 1, 2). \end{gathered} \tag{8}$$

The components of N_j parallel to the X_j and Z_j axes, respectively, are given by

$$N_{Xj} = N_j \cos \phi_j, \quad N_{Zj} = N_j \sin \phi_j. \tag{9}$$

The axis along the centerline of the deck is X. The vertical displacement and twist angle of the deck are $Y(X, T)$ and $\theta(X, T)$, respectively, with the initial (equilibrium) shape $Y_o(X)$ assumed to be a quadratic function, and the initial twist to be zero.

4.3. Equations of motion

The equations of motion for the dynamic displacements of the deck are assumed to be

$$\frac{W_D}{g} \frac{\partial^2 Y_d}{\partial T^2} + E_D I_D \frac{\partial^4 Y_d}{\partial X^4} + K(2Y_d - Z_{1d} - Z_{2d} + 2H \cos \theta_d - 2H) = F_y, \tag{10}$$

$$\begin{aligned} I_p \frac{\partial^2 \theta_d}{\partial T^2} + E_D I_w \frac{\partial^4 \theta_d}{\partial X^4} - G_D J_D \frac{\partial^2 \theta_d}{\partial X^2} - 1.5 E_D I_n \left(\frac{\partial \theta_d}{\partial X}\right)^2 \frac{\partial^2 \theta_d}{\partial X^2} \\ + K(Z_{1d} - Z_{2d} + 2D \sin \theta_d) D \cos \theta_d = M_\theta. \end{aligned} \tag{11}$$

Here K is the stiffness of the hangers on one edge of the deck (per unit length along the deck), g is gravitational acceleration, and F_y and M_θ are, respectively, the vertical force and pitching moment per unit length along the deck (due to structural damping and aerodynamic excitation).

Based on geometry and dynamic equilibrium, the governing equations for the coordinates and for the axial force components of cable j are

$$\frac{\partial X_j}{\partial S_j} = \cos \phi_j; \quad \frac{\partial Z_j}{\partial S_j} = \sin \phi_j, \quad \frac{\partial N_{Xj}}{\partial S_j} = W_C \frac{\partial^2 X_{jd}}{\partial T^2}, \tag{12,13,14}$$

$$\frac{\partial N_{Zj}}{\partial S_j} = W_C + \frac{1}{2} W_D \frac{\partial X_j}{\partial S_j} + \frac{W_C}{g} \frac{\partial^2 Z_{jd}}{\partial T^2} - K(Y_d \pm D \sin \theta_d - Z_{jd} + H \cos \theta_d - H). \tag{15}$$

In the second term in parentheses in Eq. (15), the plus sign is for cable 2 and the minus sign is for cable 1. The inextensibility condition for cable j is given by

$$\left(\frac{\partial X_j}{\partial S_j}\right)^2 + \left(\frac{\partial Z_j}{\partial S_j}\right)^2 = 1. \tag{16}$$

Also, Eqs. (9), (12), and (13) lead to the following condition, since the resultant force in each cable acts along the cable tangent:

$$N_{Xj}\frac{\partial Z_j}{\partial S_j} = N_{Zj}\frac{\partial X_j}{\partial S_j}. \tag{17}$$

The analysis is conducted in terms of the following nondimensional quantities:

$$y_d = \frac{Y_d}{D}, \quad x_j = \frac{X_j}{D}, \quad z_j = \frac{Z_j}{D} \quad s_j = \frac{S_j}{D}, \quad h = \frac{H}{D}, \quad l = \frac{L_C}{D}, \quad a = \frac{l}{2}, \quad l_H = \frac{L_H}{D}, \quad \sigma = \frac{L_C}{L},$$
$$t = T\sqrt{\frac{g}{D}}, \quad \omega = \Omega\sqrt{\frac{D}{g}}, \quad k = \frac{KD}{W_D}, \quad f_y = \frac{F_y}{W_D}, \quad m_\theta = \frac{M_\theta}{W_D D}, \quad n_j = \frac{N_j}{W_D D}, \quad n_{xj} = \frac{N_{Xj}}{W_D D},$$
$$n_{zj} = \frac{N_{Zj}}{W_D D}, \quad \lambda = \frac{\sigma^4 E_D I_D}{W_D D^3}, \quad i_P = \frac{I_P g}{W_D D^2}, \quad i_w = \frac{\sigma^4 E_D I_w}{W_D D^5}, \quad g_D = \frac{\sigma^2 G_D J_D}{W_D D^3}, \quad i_n = \frac{1.5\sigma^4 E_D I_n}{W_D D^5},$$
$$w_C = \frac{W_C}{W_D}. \tag{18}$$

In Eqs. (18), σ is the ratio of the equilibrium cable length to the span length, and is determined from the subsequent equilibrium analysis. For simplicity, the coordinate along the span is assumed to be proportional to the arc length along the cables, so that $X = S/\sigma$ and $x = s/\sigma$ where the subscript j is deleted on the arc length.

The values for the nondimensional parameters are as follows:

$$l = 146.18, \quad a = 73.09, \quad \sigma = 1.018, \quad h = 0.205, \quad \omega = 0.978, \quad \lambda = 2527,$$
$$i_P = 0.4744, \quad i_w = 2527, \quad g_D = 0.03845, \quad i_n = 367,500, \quad w_C = 0.1674. \tag{19}$$

In dimensional terms, the initial height of the deck is assumed to be

$$Y_o(S) = 4\Delta_o S(L_C - S)/(L_C^2). \tag{20}$$

The vertical equilibrium length of the hanger model at S is given by

$$L_H(S) = \Delta_o + L_o + L_1 - Y_o(S) - |Z_e(S)|. \tag{21}$$

Letting the spacing between sets of hangers be denoted D_H, the stiffness per unit length of the hanger continuum along one edge of the deck is

$$K(S) = 4E_H A_H/[D_H L_H(S)]. \tag{22}$$

The nondimensional equations of motion for the deck have the form

$$\frac{\partial^2 y_d}{\partial t^2} + \lambda\frac{\partial^4 y_d}{\partial s^4} + k(2y_d - z_{1d} - z_{2d} + 2h\cos\theta_d - 2h) = f_y, \tag{23}$$

$$i_p\frac{\partial^2\theta_d}{\partial t^2} + i_w\frac{\partial^4\theta_d}{\partial s^4} - g_D\frac{\partial^2\theta_d}{\partial s^2} - i_n\left(\frac{\partial\theta_d}{\partial s}\right)^2\frac{\partial^2\theta_d}{\partial s^2} + k(z_{1d} - z_{2d} + 2\sin\theta_d)\cos\theta_d = m_\theta. \tag{24}$$

The governing nondimensional equations for the cables are

$$\frac{\partial n_{xj}}{\partial s_j} = w_C\frac{\partial^2 x_j}{\partial t^2}, \tag{25}$$

$$\frac{\partial n_{zj}}{\partial s_j} = w_C + \frac{1}{2}\frac{\partial x_j}{\partial s_j} + w_C\frac{\partial^2 z_j}{\partial t^2} - k(y_d \pm \sin\theta_d - z_{jd} + h\cos\theta_d - h), \tag{26}$$

$$\left(\frac{\partial x_j}{\partial s_j}\right)^2 + \left(\frac{\partial z_j}{\partial s_j}\right)^2 = 1, \tag{27}$$

$$n_{xj}\frac{\partial z_j}{\partial s_j} = n_{zj}\frac{\partial x_j}{\partial s_j}. \tag{28}$$

Eqs. (23), (24), and (25)–(28) with $j = 1$ and 2 comprise a set of 10 coupled, nonlinear, partial differential equations governing the dynamic behavior of the central span.

4.4. Equilibrium solution

For equilibrium, the subscript j is deleted, f_y and m_θ are zero, the dynamic components of the variables are zero, and the accelerations are zero. From Eqs. (25) and (26),

$$n_{xe} = \text{constant}, \quad \frac{dn_{ze}}{ds} = w_C + \frac{1}{2}\frac{dx_e}{ds}. \tag{29}$$

With the use of Eqs. (27) and (28), one can obtain an equation only involving the vertical tension component $n_{ze}(s)$ and the constant horizontal tension component n_{xe}:

$$\frac{dn_{ze}}{ds} = w_C + \frac{n_{xe}}{2\sqrt{n_{xe}^2 + n_{ze}^2}}. \tag{30}$$

To compute the equilibrium shapes of the cables, instead of using Eq. (30), it is convenient to use the equilibrium equations involving the total tension $n_e(s)$ and the cable rotation $\phi_e(s)$:

$$\frac{dx_e}{ds} = \cos\,\phi_e, \quad \frac{dz_e}{ds} = \sin\,\phi_e, \quad n_e\frac{d\,\phi_e}{ds} = \left(w_C + \frac{1}{2}\cos\,\phi_e\right)\cos\,\phi_e, \quad \frac{dn_e}{ds} = \left(w_C + \frac{1}{2}\cos\,\phi_e\right)\sin\,\phi_e. \tag{31}$$

A shooting method was applied using Mathematica on the right half of a cable, with a new arc length whose origin was at the cable midpoint. The half arc length a and the tension at the midpoint were varied until the nondimensional "end conditions" of the half span horizontal length being 71.79 and the cable sag being 11.90 were satisfied with sufficient accuracy. The solution gave the values of l, a, and σ in Eqs. (19), along with the value of n_{xe}, and led to the approximate formulas

$$\begin{aligned}
z_e(s) &= -11.9 + 2.2276\times10^{-3}(s-a)^2,\\
x_e(s) &= s - 3.317\times10^{-6}(s^3 - 3as^2 + 3a^2s),\\
k(s) &= \frac{500}{l_H(s)}, \quad l_H(s) = 0.2564 + 0.0024(s-a)^2,\\
n_{xe} &= 144.9, \quad n_{ze}(s) = 0.667054(s-a) - 1.56917\times10^{-6}(s-a)^3,\\
\phi_e(0) &= -18.38^\circ = -0.3207\ \text{rad}.
\end{aligned} \tag{32}$$

In Eqs. (32), the vertical equilibrium shape of the cables is approximated by a quadratic function of the arc length. The total cable tension n_e varies from 152.7 at the towers to 144.9 at midspan. The distributed hanger stiffness $k(s)$ along one edge is plotted in Fig. 14. It ranges from about 38 at the ends to about 1950 at midspan.

4.5. Torsional oscillations of central span

Eqs. (23)–(28) are considered. They involve 10 variables: the coupled vertical and torsional motions of the deck, and the vertical and horizontal components of the motions and tensions of the cables. The variables are written in a form such as in Eqs. (8), with an equilibrium part and a dynamic part. For example, the vertical motion of cable 1 is written as $z_e(s) + z_{1d}(s,t)$. The equilibrium functions are known from Eqs. (20) and (32), along with $\theta_e = 0$.

The observed features of the predominant motion of the Tacoma Narrows Bridge during its final hour are utilized. The dimensional frequency of 0.2 Hz gives $\omega = 0.978$. The slippage amplitude of 0.51 m (1.67 ft) at the midspan of cable 2 means that the amplitude of x_{2d} at $s = a$ is 0.08547. The maximum amplitude of θ_d is 35° (0.61 rad). The cables are assumed to have no vertical displacement at the tops of the towers. Their vertical

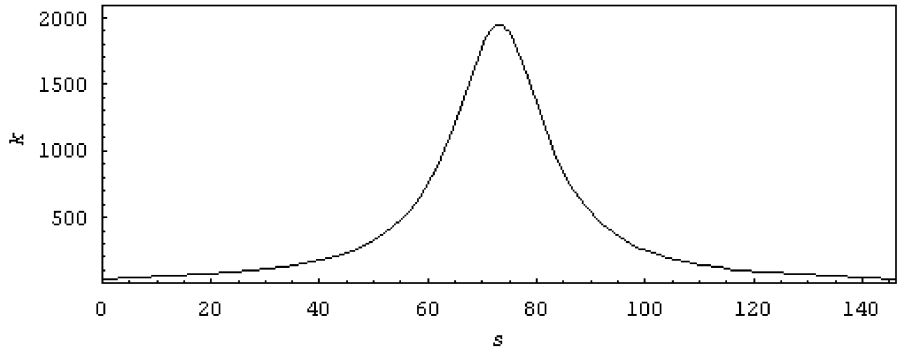

Fig. 14. Hanger stiffness versus arc length.

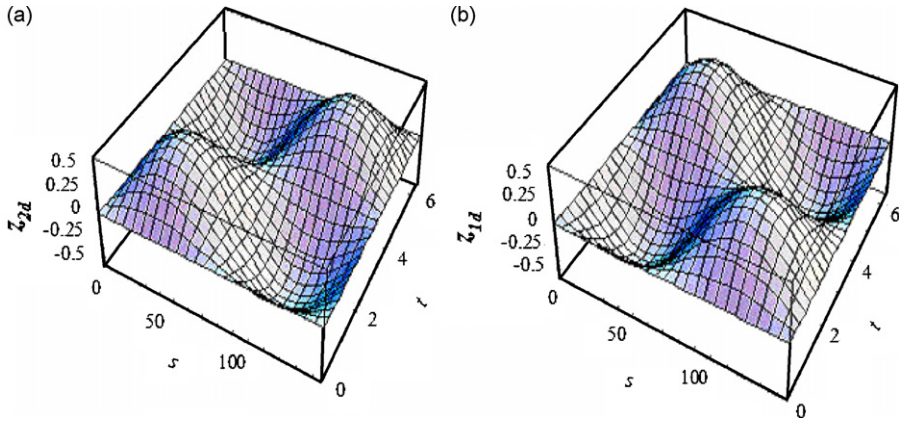

Fig. 15. Vertical components of motions of cables for one period: (a) cable 2 and (b) cable 1.

motions (from equilibrium) are assumed to be out of phase with each other and to be given by

$$z_{2d}(s_2,t) = z_o \sin\left(\frac{\pi s_2}{a}\right) \sin\,\omega t, \quad z_{1d}(s_1,t) = -z_{2d}(s_1,t). \tag{33}$$

These functions are plotted for one cycle in Fig. 15, using the amplitude z_o that will be chosen later to give the maximum twist angle of 35°. Both arc lengths are denoted s, with $0<s<146.18$. The nondimensional period of the motion is 6.425.

The shape of cable 2 is assumed to be similar to that shown in Fig. 6, so that x_{2d} is zero at the ends of the span and has magnitude 0.08547 at the center. A similar motion must have been exhibited by cable 1, despite the fact that there was no slippage. Steinman [21] conjectured that "side-span participation" or tower motions could have allowed this to happen. Extensibility of the cables, slipping of the cables over the saddles, vertical motion of the deck at midspan, and lateral motions could also have been factors. It is assumed here that the main contribution was twisting of the tops of the towers. Tower twist is described in Ref. [86] for suspension bridges in general, and in Ref. [87] with respect to the Tacoma Narrows Bridge. Shortly after the collapse, Averill [13] wrote that the two legs of each tower twisted and moved opposite to each other during the torsional motion of the deck. Here the horizontal dynamic displacement x_{1d} is assumed to be zero at midspan and to have an amplitude of 0.08547 at its ends. The assumptions for x_{1d} and x_{2d} correspond to a twist amplitude of the tops of the towers of 2.45° (0.043 rad) when viewed from above (along with bending with a longitudinal amplitude of 0.08547/2).

To obtain an approximate formula for the horizontal dynamic displacement x_{2d} of cable 2, the inextensibility condition is utilized. The expression $x_2 = x_e + x_{2d}$ is substituted into Eq. (27) with $j = 2$, and the squared terms are expanded. Then dx_e/ds_2 is approximated by unity, and the squares of the derivatives of z_e

and z_{2d} with respect to s are neglected compared to the linear terms in the dynamic variables. The result is

$$\frac{\partial x_{2d}}{\partial s_2} = \frac{dz_e}{ds_2}\frac{\partial z_{2d}}{\partial s_2}. \tag{34}$$

Eq. (34) is integrated with respect to s_2. The resulting form is used for x_{2d}, and the amplitude at midspan is chosen to be 0.08547. The resulting function, along with the corresponding function x_{1d} obtained by changing the sign of x_{2d} and shifting so that its midspan amplitude is zero, are

$$\begin{aligned} x_{2d}(s_2,t) &= -8\times10^{-6}a\left[a\cos\left(\frac{\pi s_2}{a}\right)+\pi(s_2-a)\sin\left(\frac{\pi s_2}{a}\right)-a\right]\sin\,\omega t,\\ x_{1d}(s_1,t) &= 0.08547\,\sin\,\omega t - x_{2d}(s_1,t). \end{aligned} \tag{35}$$

These functions satisfy the inextensibility condition approximately.

Fig. 16 depicts the horizonal dynamic cable displacements given in Eq. (35). Their shapes at $t = 1.606$ (one-quarter of the period of motion) are shown in Fig. 17. For cable 2, the displacement is zero at the towers, and its maximum value is not at midspan, but is 0.110 at $s = 36.5$ and 109.6. Cable 1 exhibits its maximum dynamic horizontal motion at the towers.

Next, the dynamic horizontal tension components in the cables are obtained by integration of Eq. (25), after using Eqs. (32) for the equilibrium cable forces, and Eqs. (35). This leads to

$$\begin{aligned} n_{x2d}(s_2,t) &= 8\times10^{-6}w_C\omega^2a^2\left[\frac{2a}{\pi}\sin\left(\frac{\pi s_2}{a}\right)+(a-s_2)\cos\left(\frac{\pi s_2}{a}\right)-s_2\right]\sin\,\omega t,\\ n_{x1d}(s_1,t) &= -0.08547w_C\omega^2\,\sin\,\omega t - n_{x2d}(s_1,t). \end{aligned} \tag{36}$$

The dynamic vertical tension components are computed with the use of Eq. (28). The expressions for n_{z2d} and n_{z1d}, determined with Mathematica, are extremely complicated. The total dynamic tension in each cable can then be obtained from these components, and the results, $n_{2d}(s,t)$ and $n_{1d}(s,t)$, are plotted in Fig. 18 for one period of motion. They are out of phase with each other, and their maximum values are 1.08, i.e., less than 1% of the tension at equilibrium. In dimensional terms, the maximum static tension is 56,600 kN (12.7×10^6 lb) and the maximum additional tension due to the motion is 400 kN (90,000 lb).

The twist angle of the deck is obtained by subtracting the two equations in Eq. (26), $j = 1$ and 2, from each other. After making use of Eqs. (33) and (35), this results in

$$\sin\,\theta_d = \frac{1}{2k}\left[\frac{\partial n_{z1d}}{\partial s}-\frac{\partial n_{z2d}}{\partial s}+\frac{\partial x_{2d}}{\partial s}+2(k-w_C\omega^2)z_{2d}\right]. \tag{37}$$

The amplitude z_o in Eq. (33) is now chosen to be 0.57 so that the maximum value of θ_d is 35°. To find the vertical displacement of the centerline of the deck, the two equations in Eq. (26) are added, which yields, after

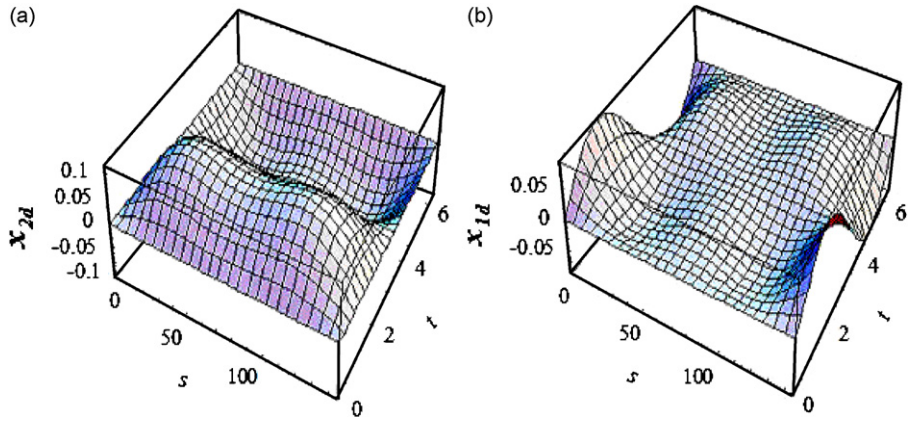

Fig. 16. Horizontal in-plane components of motions of cables for one period: (a) cable 2 and (b) cable 1.

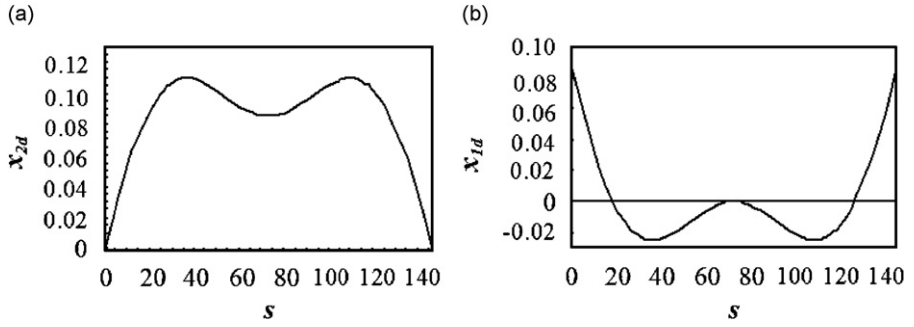

Fig. 17. Horizontal in-plane components of motions of cables versus arc length when $t = \pi/(2\omega)$: (a) cable 2 and (b) cable 1.

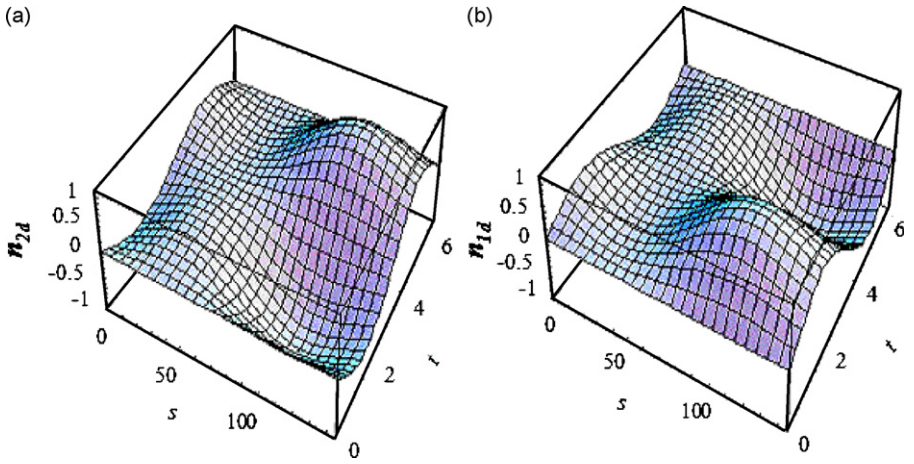

Fig. 18. Dynamic tension in cables for one period: (a) cable 2 and (b) cable 1.

using Eqs. (29), (33), and (35),

$$y_d = \frac{1}{2k}\left[2kh(1-\cos\theta_d) - \frac{\partial n_{z2d}}{\partial s} - \frac{\partial n_{z1d}}{\partial s}\right]. \tag{38}$$

The resulting functions for the twist angle $\theta_d(s,t)$ and the displacement $y_d(s,t)$ are plotted for one period in Fig. 19.

If the deck were clamped at the towers, then y_d, θ_d, and their first partial derivatives with respect to s would be zero at $s = 0$ and l. The last condition comes from the use of nonuniform torsion and the longitudinal displacement at the towers being zero [88]. These boundary conditions were not utilized in the procedure above. In the results, the maximum magnitudes of y_d, θ_d, and their first partial derivatives with respect to s at the ends of the central span are 0.00030, 0.00010, 0.00093, and 0.025, respectively. The maximum magnitude of θ_d at midspan is 1.09×10^{-6}.

The shape of the plot for θ_d in Fig. 19(a) is similar to that for z_{2d} in Fig. 15(a), although the boundary conditions are not the same. The vertical displacement y_d in Fig. 19(b) has a completely different shape from the other functions. Its amplitude is only 0.037, though, corresponding to a dimensional amplitude of 0.21 m (0.71 ft). Due to the assumed shapes for the vertical cable displacements in Eq. (33), the solution here is dominated by torsion, and the flexural motion of the deck is very small. However, the maximum vertical displacement of the edges of the deck, from equilibrium, is 4.2 m (14 ft) in this solution, as observed during the hour before the collapse.

The nondimensional resultant vertical force $f_y(s,t)$ per unit length along the centerline of the deck due to the damping and aerodynamic effects is computed from Eq. (23). The result is plotted in Fig. 20. The force is

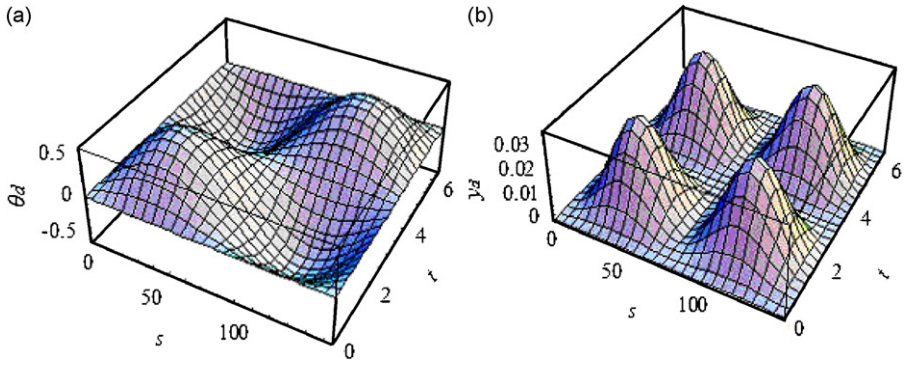

Fig. 19. Deck motions for one cycle: (a) twist angle and (b) vertical motion of centerline.

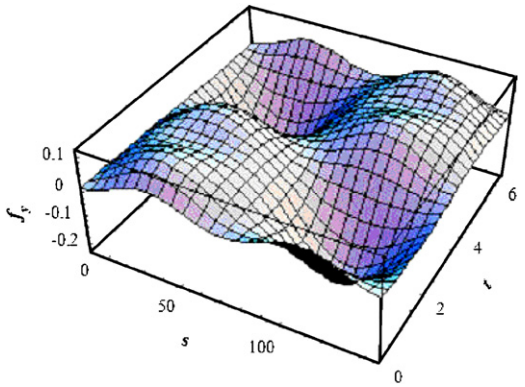

Fig. 20. Resultant vertical force on deck per unit length, due to damping and aerodynamic excitation.

positive if acting upward on the deck. Its maximum value is 0.116 and its minimum value is −0.229, corresponding in dimensional terms to 7.3 kN/m (495 lb/ft) and −14.4 kN/m (−977 lb/ft), respectively. Hence the largest downward force is about twice as big as the largest upward force.

Finally, the nondimensional resultant pitching moment m_θ per unit length along the deck is determined from Eq. (24). In addition, the approximate pitching moment $m_{\theta A}$ obtained from Eq. (24) without the second, third, and fourth terms is computed (i.e., assuming that the torsional stiffness of the deck is negligible compared to the torsional moment due to the hangers and the rotational inertia of the deck). These functions are plotted in Fig. 21, and represent the combined moment due to damping and aerodynamic effects.

The maximum amplitude of m_θ is 0.204, corresponding to a dimensional value of 75.6 kN m/m (17,000 lb ft/ft). The maximum amplitude of $m_{\theta A}$ is 0.212. Even though the maximum values are close, the shapes of the functions are quite different.

During this limit cycle, the moment m_θ is out of phase with the twist angle θ_d (see Figs. 19(a) and 21(a)) and with the rate of change of the twist angle. Except near the ends of the span ($s = 0, l$), the shape of the moment $m_\theta(s, t)$ in Fig. 21(a) has some resemblance to the shape of the fifth power of $-\theta_d(s, t)$, or, with a phase lag, to the shape of the fifth power of $\theta_d(s, t-0.5t_f)$ where t_f is the period $2\pi/\omega$. The shape of $m_\theta(s, t)$ also resembles the shape of the fifth power of $\beta(s,t–0.75t_f)$ where $\beta = \partial\theta_d/\partial t$.

The structural damping in the original Tacoma Narrows Bridge was much lower than that in typical suspension bridges [13]. Therefore the functions f_y and m_θ may be dominated by wind effects, including aerodynamic damping. Since the functions are not zero at the ends of the central span, they cannot be written as a power series in the deck's displacements and velocities if those variables are zero at the towers, without including a term that is independent of those variables.

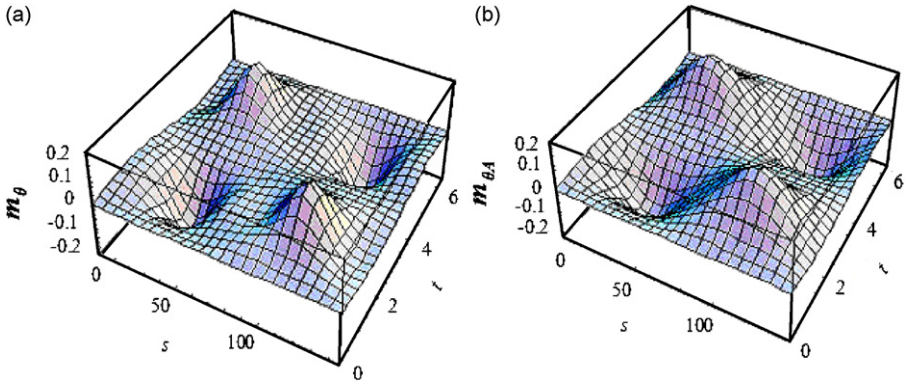

Fig. 21. Resultant pitching moment on deck per unit length, due to damping and aerodynamic excitation: (a) including torsional stiffness of deck and (b) neglecting torsional stiffness of deck.

5. Concluding remarks

The original Tacoma Narrows Bridge exhibited vertical oscillations from the time that it was constructed, but these oscillations did not cause any significant damage. The bridge was stable with respect to torsional motion until the north midspan cable band loosened, allowing the north suspension cable to move longitudinally through it. The loosening of the cable band was probably due in part to snap loads in the two diagonal ties that connected the band to the plate girder along the edge of the deck. This led to about 700 cycles of torsional oscillation for approximately 1 hour until the deck broke up and the central span collapsed. The behavior of the cable band just prior to torsional motion, and the subsequent steady-state torsional oscillations, were considered here.

Models for the tie forces were described in Section 2. Then a continuum model was formulated in Section 3 for the deck, suspension cables, and hangers in the main span. Making use of the known conditions during the torsional oscillations and some assumed shapes for the cable motions, an approximate solution was obtained in Section 4 for the cable tension, deck motion, and resultant force and moment acting on the deck due to damping and aerodynamic excitation.

The shift from vertical to torsional oscillations was not due to an increase in wind speed. Also, it was not due to a nonlinear system switching from one limit cycle to another, as conjectured in some previous analyses. Instead, the system changed, and the local reduction of frictional resistance in the north midspan cable band allowed torsional motion to be initiated. The flutter response quickly went into a limit cycle that was dominated by torsion of the deck.

A linear analysis is not adequate to describe this motion. The rotational stiffness of the deck cannot be modeled only by linear terms for uniform and nonuniform torsion. The aerodynamic forces and moments cannot be modeled simply as linear functions of the displacements and velocities. In the analysis presented here, the combined aerodynamic and damping effects were determined from the known properties of the motion (i.e., an inverse approach was utilized). The continuum model for the central span was more general than previous models in various aspects, and included large twist angles of the deck, large motions of the cables, transverse and longitudinal inertias of the cables, and hanger stiffnesses that varied along the deck.

It was assumed that the motion of the south cable involved longitudinal displacements associated with twisting of the towers. For the north cable, longitudinal slippage of the cable with an amplitude of 0.51 m (1.67 ft) at midspan was modeled. The other cable bands apparently did not show evidence of slippage. The longitudinal motions of those bands, required for the motions of the cables during torsion, were probably accommodated largely by rotation of the hangers in their vertical plane. For example, the set of hangers adjacent to midspan had a vertical length of about 1.6 m (5.3 ft). To handle a longitudinal (horizontal) amplitude of about 0.5 m (1.6 ft) would require a rotation of these hangers (in the vertical plane) of about 17° (0.3 rad). Extensibility of the hangers and longitudinal motion of the deck may have assisted in allowing the required longitudinal motions of the cable bands and reduced such rotations of the hangers.

The bridge was the third longest suspension bridge in the world at the time. Relative to similar bridges, it was very light, slender, and flexible, and in particular had low torsional stiffness. The midspan diagonal ties were flexible and insufficiently pretensioned. The cable bands were lighter than those used in previous bridges. The US government's desire to spend significantly less money on the bridge than estimated for the initial design was the motivation for the radical design of the deck. The result was disastrous, but led to new investigations and understanding of the dynamic behavior of long-span suspension bridges.

Acknowledgments

This material is based upon work supported by the US National Science Foundation under Grant no. 0114709. The author is grateful to Richard S. Hobbs for considerable assistance regarding the history of the bridge, to Richard Scott for some very useful information, and to Hannah Palin and her colleagues for help in the author's study of the archival films and the F. B. Farquharson papers at the Special Collections Division of the University of Washington Libraries. Also, the author thanks the reviewers for their helpful comments.

References

[1] O.H. Ammann, T. von Kármán, G.B. Woodruff, The failure of the Tacoma Narrows Bridge: a report to the Honorable John M. Carmody, Administrator, Federal Works Agency, Washington, DC, March 28, 1941. Also in: *The Failure of the Tacoma Narrows Bridge: A Reprint of Original Reports, Advisory Board on the Investigation of Suspension Bridges*, Bulletin No. 78 of the Agricultural and Mechanical College of Texas, Fourth Series, Vol. 15, No. 1, School of Engineering, Texas Engineering Experiment Station, College Station, Texas, January 1, 1944.

[2] F.B. Farquharson, Aerodynamic stability of suspension bridges with special reference to the Tacoma Narrows Bridge, Part I—Investigations prior to October 1941, Bulletin No. 116, University of Washington Engineering Experiment Station, 1949.

[3] F.C. Smith, G.S. Vincent, Aerodynamic stability of suspension bridges with special reference to the Tacoma Narrows Bridge, Part II—Mathematical analyses, Bulletin No. 116, University of Washington Engineering Experiment Station, 1950.

[4] F.B. Farquharson, Aerodynamic stability of suspension bridges with special reference to the Tacoma Narrows Bridge, Part III—The investigation of models of the original Tacoma Narrows Bridge under the action of wind, Bulletin No. 116, University of Washington Engineering Experiment Station, 1952.

[5] F.B. Farquharson, Aerodynamic stability of suspension bridges with special reference to the Tacoma Narrows Bridge, Part IV—Model investigations which influenced the design of the new Tacoma Narrows Bridge, Bulletin No. 116, University of Washington Engineering Experiment Station, 1952.

[6] G.S. Vincent, Aerodynamic stability of suspension bridges with special reference to the Tacoma Narrows Bridge, Part V—Extended studies: Logarithmic decrement, field damping, prototype predictions, four other bridges, Bulletin No. 116, University of Washington Engineering Experiment Station, 1954.

[7] R. Scott, *In the Wake of Tacoma*, American Society of Civil Engineers, Reston, VA, 2001.

[8] R.S. Hobbs, *Catastrophe to Triumph: Bridges of the Tacoma Narrows*, Washington State University Press, Pullman, WA, 2006.

[9] http://www.wsdot.wa.gov/TNBhistory.

[10] http://www.lib.washington.edu/specialcoll/exhibits/tnb/.

[11] http://search.tpl.lib.wa.us/images/dt3.asp.

[12] K.Y. Billah, R.H. Scanlan, Resonance, Tacoma Narrows Bridge failure, and undergraduate physics textbooks, *American Journal of Physics* 59 (1991) 118–124.

[13] W.A. Averill, Collapse of the Tacoma Narrows Bridge, *Pacific Builder and Design* 46 (12/1940) 20–27.

[14] M. Levy, M. Salvadori, *Why Buildings Fall Down*, W.W. Norton & Company, New York, 2002 (Chapter 7).

[15] C.E. Paine, H. Cross, S. Hardesty, H.D. Robinson, W.M. Wilson, The failure of the suspension bridge over Tacoma Narrows, Report to the Narrows Bridge Loss Committee (Paul Carew, Chairman) on the damage produced by the failure, June 2, 1941, Seattle, WA, in: *The Failure of the Tacoma Narrows Bridge: A Reprint of Original Reports*, Advisory Board on the Investigation of Suspension Bridges, Bulletin No. 78 of the Agricultural and Mechanical College of Texas, Fourth Series, Vol. 15, No. 1, School of Engineering, Texas Engineering Experiment Station, College Station, Texas, January 1, 1944.

[16] L.J. Sverdrup, F. Donaldson, R.G. Cone, Report of the Board of Investigation, Tacoma Narrows Bridge: Part I, Amount of Loss (2/3/41); Part II, Cause of Collapse (6/26/41); Part III, Special Report on Main Towers (6/26/41), in: *The Failure of the Tacoma Narrows Bridge: A Reprint of Original Reports*, Advisory Board on the Investigation of Suspension Bridges, Bulletin No. 78 of the Agricultural and Mechanical College of Texas, Fourth Series, Vol. 15, No. 1, School of Engineering, Texas Engineering Experiment Station, College Station, Texas, January 1, 1944.

[17] C.H. Eldridge, The Tacoma Narrows Bridge, *Civil Engineering (ASCE)* 10 (5/1940) 299–302.

[18] H.F. Donnelly, *Report on the Construction of the Superstructure*, Tacoma Narrows Bridge Collection, Washington State Archives, Olympia, WA, 1940.

[19] M. Brumer, H. Rothman, M. Fiegen, B. Forsyth, Verrazano-Narrows Bridge: design of superstructure, *Journal of the Construction Division (ASCE)* 92 (CO1) (1966) 23–70.
[20] A. Bowers, Model tests showed aerodynamic instability of Tacoma Narrows Bridge, *Engineering News-Record* 125 (11/21/1940) 44–47.
[21] D.B. Steinman, Rigidity and aerodynamic stability of suspension bridges, *Transactions of the American Society of Civil Engineers* 110 (1945) 439–475 (discussion 476–580).
[22] V.I. Babitsky, *Theory of Vibro-Impact Systems and Applications*, Springer, Berlin, 1998.
[23] B. Brogliato, *Nonsmooth Mechanics: Models, Dynamics, and Control*, Springer, London, 1999.
[24] H. Luo, S. Hanagud, On the dynamics of vibration absorbers with motion-limiting stops, *Journal of Applied Mechanics* 65 (1998) 223–233.
[25] E.A. Butcher, D.J. Segalman, Characterizing damping and restitution in compliant impacts via modified K–V and higher-order linear viscoelastic models, *Journal of Applied Mechanics* 67 (2000) 831–834.
[26] A. Narimani, M.F. Golnaraghi, G. Nakhaie Jazar, Sensitivity analysis of the frequency response of a piecewise linear system in a frequency island, *Journal of Vibration and Control* 10 (2004) 175–198.
[27] A.L. Farmer, R.H. Plaut, M.M. Holland, Bouncing-ball model of "dry" motions of a tethered buoy, *Journal of Vibration and Acoustics* 123 (2001) 333–339.
[28] R.H. Plaut, W.T. Fielder, L.N. Virgin, Fractal behavior of an asymmetric rigid block overturning due to harmonic motion of a tilted foundation, *Chaos, Solitons & Fractals* 7 (1996) 177–196.
[29] S. Wolfram, *The Mathematica Book*, third ed., Cambridge University Press, Cambridge, UK, 1996.
[30] H.M. Lankarani, P.E. Nikravesh, A contact force model with hysteresis damping for impact analysis of multibody systems, *Journal of Mechanical Design* 112 (1990) 369–376.
[31] G. Wegener, R. Markert, Influence of contact and impacts on the dynamics of an elastic rotor with an elastic retainer bearing, in: V.I. Babitsky (Ed.), *Dynamics of Vibro-Impact Systems*, Springer, Berlin, 1999, pp. 89–98.
[32] R. Jankowski, Non-linear viscoelastic modelling of earthquake-induced structural pounding, *Earthquake Engineering and Structural Dynamics* 34 (2005) 595–611.
[33] T.C. Kim, T.E. Rook, R. Singh, Effect of nonlinear impact damping on the frequency response of a torsional system with clearance, *Journal of Sound and Vibration* 281 (2005) 995–1021.
[34] S. Muthukumar, R. Desroches, A Hertz contact model with non-linear damping for pounding simulation, *Earthquake Engineering and Structural Dynamics* 35 (2006) 811–828.
[35] S. Abrate, R. Dooley, R. Kaste, G. Thibault, W. Millette, Nonlinear dynamic behavior of parachute static lines, *Composite Structures* 61 (2003) 3–12.
[36] C.M. Hennessey, N.J. Pearson, R.H. Plaut, Experimental snap loading of synthetic ropes, *Shock and Vibration* 12 (2005) 163–175.
[37] J.C. Ryan, Analytical and Experimental Investigation of Improving Seismic Performance of Steel Moment Frames Using Synthetic Fiber Ropes, PhD Dissertation, Virginia Tech, Blacksburg, VA, 2006 ⟨http://scholar.lib.vt.edu/theses/available/etd-10282006-094904/⟩.
[38] R.H. Plaut, F.M. Davis, Sudden lateral asymmetry and torsional oscillations of section models of suspension bridges, *Journal of Sound and Vibration*, to appear.
[39] A.C. Lazer, P.J. McKenna, Large-amplitude periodic oscillations in suspension bridges: some new connections with nonlinear analysis, *SIAM Review* 32 (1990) 537–578.
[40] Y.S. Choi, K.C. Jen, P.J. McKenna, The structure of the solution set for periodic oscillations in a suspension bridge model, *IMA Journal of Applied Mathematics* 47 (1991) 283–306.
[41] S.H. Doole, S.J. Hogan, A piecewise linear suspension bridge model: nonlinear dynamics and orbit continuation, *Dynamics and Stability of Systems* 11 (1996) 19–47.
[42] A.R. Champneys, P.J. McKenna, On solitary waves of a piecewise linear suspended beam model, *Nonlinearity* 10 (1997) 1763–1782.
[43] L.D. Humphreys, P.J. McKenna, Multiple periodic solutions for a nonlinear suspension bridge equation, *IMA Journal of Applied Mathematics* 63 (1999) 37–49.
[44] A.R. Champneys, P.J. McKenna, P.A. Zegeling, Solitary waves in nonlinear beam equations: stability, fission and fusion, *Nonlinear Dynamics* 21 (2000) 31–53.
[45] A. Fonda, Z. Schneider, F. Zanolin, Periodic oscillations for a nonlinear suspension bridge model, *Journal of Computational and Applied Mathematics* 52 (1994) 113–140.
[46] Y. An, C. Zhong, Periodic solutions of a nonlinear suspension bridge equation with damping and nonconstant load, *Journal of Mathematical Analysis and Applications* 279 (2003) 569–579.
[47] M.S.T. de Freitas, R.L. Viana, C. Grebogi, Erosion of the safe basin for the transversal oscillations of a suspension bridge, *Chaos, Solitons & Fractals* 18 (2003) 829–841.
[48] M.S.T. de Freitas, R.L. Viana, C. Grebogi, Basins of attraction of periodic oscillations in suspension bridges, *Nonlinear Dynamics* 37 (2004) 207–226.
[49] M.S.T. de Freitas, R.L. Viana, C. Grebogi, Multistability, basin boundary structure, and chaotic behavior in a suspension bridge model, *International Journal of Bifurcation and Chaos* 14 (2004) 927–950.
[50] H. Petroski, Still twisting, *American Scientist* 79 (1991) 398–401.
[51] D. Berreby, The great bridge controversy, *Discover* 13 (2/1992) 26–33.
[52] G. Tajcová, Mathematical models of suspension bridges, *Applications of Mathematics* 42 (1997) 451–480.

[53] N.U. Ahmed, H. Harbi, Mathematical analysis of dynamic models of suspension bridges, *SIAM Journal on Applied Mathematics* 58 (1998) 853–874.
[54] N.U. Ahmed, H. Harbi, Stability of suspension bridge I: aerodynamic and structural damping, *Mathematical Problems in Engineering* 4 (1998) 73–98.
[55] Y. An, Nonlinear perturbations of a coupled system of steady state suspension bridge equations, *Nonlinear Analysis* 51 (2002) 1285–1292.
[56] Z. Ding, Nonlinear periodic oscillations in a suspension bridge system under periodic external aerodynamic forces, *Nonlinear Analysis* 49 (2002) 1079–1097.
[57] Z. Ding, Multiple periodic oscillations in a nonlinear suspension bridge system, *Journal of Mathematical Analysis and Applications* 269 (2002) 726–746.
[58] Z. Ding, Traveling waves in a suspension bridge system, *SIAM Journal on Mathematical Analysis* 35 (2003) 160–171.
[59] K.S. Moore, Large torsional oscillations in a suspension bridge: multiple periodic solutions to a nonlinear wave equation, *SIAM Journal on Mathematical Analysis* 33 (2002) 1411–1429.
[60] D. Jacover, P.J. McKenna, Nonlinear torsional flexings in a periodically forced suspended beam, *Journal of Computational and Applied Mathematics* 52 (1994) 241–265.
[61] N.U. Ahmed, H. Harbi, Torsional and longitudinal vibration of suspension bridge subject to aerodynamic forces, *Mathematical Problems in Engineering* 4 (1998) 393–421.
[62] K.S. Moore, Large Amplitude Torsional Oscillations in a Nonlinearly Suspended Beam: A Theoretical and Numerical Investigation, PhD Dissertation, University of Connecticut, Storrs, CT, 2001.
[63] J.R. Banerjee, A simplified method for the free vibration and flutter analysis of bridge decks, *Journal of Sound and Vibration* 260 (2003) 829–845.
[64] M. Como, S. Del Ferraro, A. Grimaldi, A parametric analysis of the flutter instability for long span suspension bridges, *Wind and Structures* 8 (2005) 1–12.
[65] M. Diaferio, V. Sepe, Smoothed "slack cable" models for large amplitude oscillations of suspension bridges, *Mechanics Based Design of Structures and Machines* 32 (2004) 363–400.
[66] P.J. McKenna, C. Ó Tuama, Large torsional oscillations in suspension bridges visited again: vertical forcing creates torsional response, *American Mathematical Monthly* 108 (2001) 738–745.
[67] F. Bleich, C.B. McCullough, R. Rosecrans, G.S. Vincent, *The Mathematical Theory of Vibration in Suspension Bridges*, US Government Printing Office, Washington, DC, 1950.
[68] R.H. Scanlan, J.J. Tomko, Airfoil and bridge deck flutter derivatives, *Journal of the Engineering Mechanics Division (ASCE)* 97 (1971) 1717–1737.
[69] H. Tanaka, Similitude and modelling in bridge aerodynamics, in: A. Larsen (Ed.), *Aerodynamics of Large Bridges*, A.A. Balkema, Rotterdam, 1992, pp. 83–94.
[70] T.A. Wyatt, Bridge aerodynamics 50 years after Tacoma Narrows—part I: the Tacoma Narrows failure and after, *Journal of Wind Engineering and Industrial Aerodynamics* 40 (1992) 317–326.
[71] A. Larsen, Aerodynamics of the Tacoma Narrows Bridge—60 years later, *Structural Engineering International* 4 (2000) 243–248.
[72] M. Matsumoto, H. Shirato, T. Yagi, R. Shijo, A. Eguchi, H. Tamaki, Effects of aerodynamic interferences between heaving and torsional vibration of bridge decks: the case of Tacoma Narrows Bridge, *Journal of Wind Engineering and Industrial Aerodynamics* 91 (2003) 1547–1557.
[73] T. Miyata, Historical view of long-span bridge aerodynamics, *Journal of Wind Engineering and Industrial Aerodynamics* 91 (2003) 1393–1410.
[74] D. Green, W.G. Unruh, The failure of the Tacoma Bridge: a physical model, *American Journal of Physics* 74 (2006) 706–716.
[75] F. Ehsan, R.H. Scanlan, Vortex-induced vibrations of flexible bridges, *Journal of Engineering Mechanics* 116 (1990) 1392–1411.
[76] R.H. Scanlan, Bridge flutter derivatives at vortex lock-in, *Journal of Structural Engineering* 124 (1998) 450–458.
[77] E. Simiu, R.H. Scanlan, *Wind Effects on Structures*, third ed., Wiley, New York, 1996.
[78] A. Pugsley, *The Theory of Suspension Bridges*, Edward Arnold, London, 1968.
[79] J. Jones, Welded cable saddles for Tacoma Narrows Bridge, *Engineering News-Record* 123 (12/7/1939) 91–92.
[80] N.S. Trahair, Nonlinear elastic nonuniform torsion, *Journal of Structural Engineering* 131 (2005) 1135–1142.
[81] W.T. Thomson, *Theory of Vibrations with Applications*, fourth ed., Prentice Hall, Englewood Cliffs, NJ, 1993.
[82] W. Podolny Jr., D. Goodyear, Cable-suspended bridges, in: R.L. Brockenbrough, F.S. Merritt (Eds.), *Structural Steel Designer's Handbook*, fourth ed., McGraw-Hill, New York, 2006, pp. 15.1–15.91.
[83] M. Herzog, The aerostatic stability of suspension bridges, *Schweizer Ingenieur und Architekt* 9 (1990) 223–229 (in German).
[84] J.A. Jurado, S. Hernández, Sensitivity analysis of bridge flutter with respect to mechanical parameters of the deck, *Structural and Multidisciplinary Optimization* 27 (2004) 272–283.
[85] http://www.kuleuven.ac.be/bwk/materials/Teaching/master/wg15b/l0900.htm.
[86] C. O'Connor, *Design of Bridge Superstructures*, Wiley, New York, 1971.
[87] L.G. Dunn, The influence of tower rigidity on the symmetric torsional modes of vibration, Technical Report, Graduate Aeronautical Laboratories (GALCIT), Caltech, Pasadena, CA, 1942.
[88] A. Gjelsvik, *The Theory of Thin Walled Bars*, Wiley, New York, 1981.